Advanced Computational Aeroelasticity and Multidisciplinary Application for Composite Curved Wing*1

By Dong-Hyun Kim[1)] and Yu-Sung Kim[1)]

[1)]*School of Mechanical and Aerospace Engineering,*
GyeongSang National University (GSNU), Jinju City, 660-701, Republic of Korea

This article preferentially describes advanced computational aeroelasticity and its multidisciplinary applications based on the coupled CFD and CSD method. A modal-based coupled nonlinear aeroelastic analysis system incorporated with unsteady Euler aerodynamics has been developed based on the high-speed parallel processing technique. It is clearly expected to give accurate and practical engineering data in the design fields of generic flight vehicles. Also, efficient and robust computational system for the flutter optimization has been developed using the coupled computational method with the micro genetic algorithm. Vibration and flutter characteristics of composite curved wing are also investigated in this study. Virtual flutter tests for the spanwise curved composite missile fin are effectively conducted using the present advanced computational method with high speed parallel processing technique. As computational demonstrations, the effects of ply orientation and stacking sequence on the flutter speed have been investigated and compared with the case of isotropic curved shell model with the same structural weight.

Key Words: Aeroelasticity, Flutter, CFD, CSD, Euler, Unstructured Grid, Numerical Simulation, Genetic Algorithm, Curved Wing

1. Introduction

Nowadays, the accurate prediction of flutter boundary becomes a really important technology to reduce the structural weight and to estimate its actual flight performance in the design process. The main purposes of this article are to introduce a delicate and general computational analysis system. This article preferentially describes advanced computational aeroelasticity and related numerical backgrounds based on the coupled CFD and CSD method based on the high-speed parallel processing technique. In the development of new weapon systems such as bomb, projectile, guided or unguided missile, primary emphasis should be placed on the simplicity and reliability. A weapon will have far greater reliability if it can be sealed in a container of minimum volume and geometry. The solution for this problem can be efficient solved by using a wrap around fin or simply called spanwise curved wing concept. The curved wing offers a solution for many geometric constraints and at the same time can be sized to provide aerodynamic stabilizing characteristics equal to flat wing stabilizers. Because of its unique aerodynamic characteristics and geometry shape, it is also interesting for aerospace research engineers to investigate the flutter characteristics of the curved wing model.

The composite materials since its invention have been used widely in engineering especially for aircraft structures because of its advantage compared to the conventional engineering materials. Composite materials have many characteristics that are different from the conventional engineering materials such as high specific strength and directional stiffness. Use of all the characteristics advantage allows the tailoring of composite materials to meet a particular structural requirement. It is well-known that the optimum design of wing can be achieved by aeroelastic tailoring of composite wing structures[1-7)]. However, it is hard to find previous research works for the flutter analysis of composite curved wing shapes.

Nowadays, the accurate prediction of flutter boundary becomes a really important one to reduce the structural weight and to estimate its actual flight performance in the design process. This paper has focus on the compressible flutter analyses for the laminated composite curved wing. It also describes the development of a delicate and general computational analysis system and to exactly consider the effect of curved wing configuration. In this study, a modal-based numerical flutter analysis system in the time domain has been developed including the physical matched point concept. The parallel unstructured Euler solver was adopted and newly modified to be coupled with the dynamic aeroelastic solver. Finally, efficient and robust computational system for the flutter optimization has been developed using the coupled computational method with the micro genetic algorithms. Structural free vibration analyses have been performed using finite element method. Detailed nonlinear time responses are computed by the simultaneous coupled time-integration method in the compressible flow regions. Various computational results are presented and investigated in detail.

2. Unsteady Aerodynamic Modeling

The compressible Euler equations can be written in an integral form over a control volume V moving with a velocity $\vec{V}_g$.

$$\frac{\partial}{\partial t}\int_V Q dV + \oint_S F(Q)\cdot\vec{n} dS = 0 \tag{1}$$

where

$$Q = \begin{pmatrix} \rho \\ \rho u \\ \rho v \\ \rho w \\ e_0 \end{pmatrix}, \quad F(Q,\vec{n}) = \begin{pmatrix} \rho\bar{u} \\ \rho u\bar{u} + pn_x \\ \rho v\bar{u} + pn_y \\ pw\bar{u} + pn_z \\ e_0\bar{u} + pV_n \end{pmatrix}$$

Also,

$$\bar{u} = \vec{n}\cdot\left(\vec{V} - \vec{V}_g\right)$$
$$V_n = \vec{n}\cdot\vec{V}$$

where $\vec{V}_g$ and $\vec{n}$ are the grid velocity and the outward unit normal vector. Pressure and total enthalpy can be expressed from ideal gas relations:

*1 This is a reduced version of the presented paper at the conference.

$$p = (\gamma - 1)[e_0 - \frac{1}{2}\rho(u^2 + v^2 + w^2)] \quad (2)$$

$$h = \frac{\gamma}{(\gamma - 1)}\frac{p}{\rho} + \frac{1}{2}\rho(u^2 + v^2 + w^2) \quad (3)$$

where γ is the specific ratio.

The inviscid flux across each cell face is computed by using the Roe's flux-difference splitting formula. For high-order spatial accuracy, estimation of the state variables at each cell face is achieved by interpolating the solution with a Taylor series expansion in the neighborhood of each cell center. The cell-averaged solution gradient required at the cell center for the above expansion is computed by using the Gauss' theorem by evaluating the surface integral for the closed surface of the tetrahedrons. This process can be simplified using some geometrical invariant features of the tetrahedral. The expansion also requires the nodal value of the solution, which can be computed from the surrounding cell center data using a second-order accurate pseudo-Laplacian averaging procedure as suggested by Holmes and Connell[8].

For steady-state computations, the governing equations are linearized and advanced in time using the first-order Euler backward time integration.

$$\left[\frac{V}{\Delta\tau}I + \frac{\partial R}{\partial Q}\right]^n \Delta Q^n = -R^n \quad (4)$$

where $\Delta Q^n = Q^{n+1} - Q^n$. Also, $\Delta\tau$, R, n, and V mean the nondimensional time step, the residual, the time integration counter, and the cell volume, respectively. The nondimensional time is normalized as the reference chord length and freestream sonic speed.

For unsteady computations, Eq. (4) can be recast to include temporal numerical subiterations as a dual-time stepping. With the subiteration counter denoted by m, the solution vector Q at advancing time level n+1 is now defined as

$$\left[(\frac{V}{\Delta\tau^*} + \frac{3V}{2\Delta\tau})I + \frac{\partial R}{\partial Q}\right]^m \Delta Q^m = -R^*(Q^m) \quad (5)$$

where $\Delta Q^m = Q^{m+1} - Q^m$. Also, τ* denotes the pseudo time for the dual-time stepping and $R^*(Q^m)$ is the unsteady residual newly defined as follow:

$$R^*(Q^n) = R(Q^n) + \frac{3Q^mV^{n+1} - 4Q^nV^n + Q^{n-1}V^{n-1}}{2\Delta\tau} \quad (6)$$

The solution vector ΔQ denotes the change in state variables between numerical subiterations during a certain time step. When the subiterations drive the residual towards zero, not only second order time accuracy is achieved, but the linearization errors are also driven to zero. Typically, three to five subiterations with a certain convergence criteria per each time step are effectively used to reduce the magnitude of numerical residuals. Direct solution of the system of simultaneous equations resulting from equation for overall cells requires the inversion of a large sparse matrix, which is computationally very expensive. Thus, Gauss-Seidel relaxation method is used to iteratively solve the system of flow equations.

Furthermore, to avoid numerical errors induced by the deforming or moving mesh, the cell volumes are integrated forward in time adopting the geometric conservation law (GCL). The geometric conservation law used in this study is of the same integral form as the mass conservation law and defined by

$$\frac{\partial}{\partial\tau}\int_\Omega dV - \oint_{\partial\Omega} V_g \cdot \vec{n} d\Omega = 0 \quad (7)$$

Discretization of above equation yields

$$V_i^{n+1} = V_i^n + \Delta\tau \sum V_g \cdot \vec{n} \quad (8)$$

The local cell volumes at time level (n+1) in Eq. (6) are computed to satisfy the GCL by applying above equation at every global time step.

Parallel Implementation of the Solver

Parallelization of the Gauss-Seidel implicit scheme is fairly straightforward and has been well described in a literature[9]. The present flow solver is parallelized by partitioning the global computational domain into local subdomains. The intermediate decomposition or partitioning is performed using the MeTiS library[10]. The local domain mesh data is allocated on each processor and the calculation is performed on the local computational domain by updating the solution information among subdomain boundaries. The inter-boundaries commonly included in each subdomain are considered as artificial boundaries for data communication. To do this, ghost cells attached to these inter-boundaries for the present cell-centered scheme were also introduced. Initially, face-center values of the flow variables are interchanged through the inter-boundary faces. These values are used to calculate the flux Jacobian on the inter-boundary. Data communication among processors is achieved using the standard message passing interface (MPI) library installed on LINUX operating system. Next, the cell-center values are exchanged across the boundary during the Gauss-Seidel iteration (GSI). Boundary node values and the weighting factors for Laplacian averaging are also communicated to achieve the high-order reconstruction. In the present study, cell data are exchanged in each GSI, and face and node data are transferred for the next global iteration. Since 25~30 numerical iterations are typically required in each time step to get the local converged solution, much communication time is spent during the GSI process. Therefore, three or five times of actual communications are generally performed to reduce the communicational overhead due to the GSI.

Modified Spring Analogy for Robust Moving Grid

For the analyses on the complex moving body problems, the modified type of spring analogy technique[11] is adopted to compute the deformation of the mesh during the time integration of the fluid. In the spring analogy, the mesh is considered as fictitious springs. Boundary nodes are moved by aeroelastic computations and interior nodes are moved by the spring analogy with several iterations. In the present research, segment spring method is basically used. Here, the equilibrium lengths of the springs are equal to the initial lengths of the segments. It may be noted here that since the present moving grid technique combined with parallel processing is applied locally on each processor, the disagreement of nodes at the communication boundaries may be occurred due to the independent local iterations for the spring analogy. To avoid this kind of nonsynchronization problem, coordinates of nodes at the communication boundaries have to be also transferred into each other as the numerical constraints.

3. Aeroelastic Modeling

The governing aeroelastic equations of motion of a flexible wing are obtained by using the Rayleigh-Ritz method. In this method, the resulting aeroelastic displacement at any time can be expressed as a function of a finite set of selected modes. The

general motion of the wing assumed to be described by the separation of time and space variables as follows

$$\begin{aligned} \{u(t)\} &= [\Phi_x(x,y,z)]\{q(t)\} \\ \{v(t)\} &= [\Phi_y(x,y,z)]\{q(t)\} \\ \{w(t)\} &= [\Phi_z(x,y,z)]\{q(t)\} \end{aligned} \tag{9}$$

where {u}, {v} and {w} are the structural deflections and $[\Phi_X]$, $[\Phi_Y]$ and $[\Phi_Z]$ are the matrices of x-, y- and z-direction displacements of the natural vibration modes. Usually, the column size of modal matrix [Φ] is depends on the selection of considering natural mode in the flutter analysis.

The aeroelastic equations of motion for an elastic wing may be formulated in terms of generalized displacement response vector $\{q(t)\}$ which is a solution of the following equation:

$$[M_g]\{\ddot{q}(t)\}+[C_g]\{\dot{q}(t)\}+[K_g]\{q(t)\}=\{Q(t,q,\dot{q})\} \tag{10}$$

where t is the physical time, $[M_g]$ is the generalized mass matrix, $[C_g]$ is the generalized damping matrix, $[K_g]$ is the generalized stiffness matrix, and $\{Q\}$ is the vector of generalized aerodynamic forces computed by integrating the pressure distributions on the wing surface as

$$Q(t)_i = \frac{1}{2}\rho U^2 c_r{}^2 \iint_S -Cp(x,y,z,t)\left(n_x\psi_{xi}+n_y\psi_{yi}+n_z\psi_{zi}\right)\frac{dS}{c_r{}^2} \tag{11}$$

where ρ is the free stream air density, U is the free stream velocity, c_r is the reference chord length, S is the wing area, Cp is the unsteady pressure coefficient on the arbitrary wing surface, n_x, n_y and n_z means the surface normal vectors for x, y and z direction, respectively and ψ_i are the *i-th* natural mode shape vectors interpolated on the aerodynamic surface mesh. The generalized aerodynamic forces of Eq. (11) are integrated numerically for the wing, pylon and store configurations. In this study, to consider the characteristics of nonlinear aeroelastic responses in detail, the coupled time-marching method (CTM) has been applied.

In general, the computation time needed in solving the structural equation is much less than those required in the decomposed fluid domains. Thus, to the parallel coupling with the unsteady fluid domains, one single computer node is usually prepared for solving the structural equations. At each global time step, all the local generalized forces computed from each computer node are to be transferred into the node for structure solver. Then, the generalized displacements can be obtained and the classified data for physical moving boundary are to be transferred into the each corresponding computer nodes for spring analogy and unsteady fluid solution. In addition, this includes the staggered coupling algorithm with internal iterations to increase the temporal coupling accuracy. Data communications among computer nodes are also conducted using the standard message passing interface (MPI) library installed on a LINUX operating system.

In this study, the time marching process of the structure-fluid coupling was performed by similarly adopting the second-order staggered algorithm. It is well known that this algorithm is constructed as a leap-frog scheme where the fluid subsystem is always computed at half time-stations, while the structure subsystem is always computed at full time-stations. The road map of the numerical coupling process applied in this study is shown in Fig.1. Here, the transferred structural displacement and velocity are to be normalized to keep the numerical consistency with the normalized fluid domain.

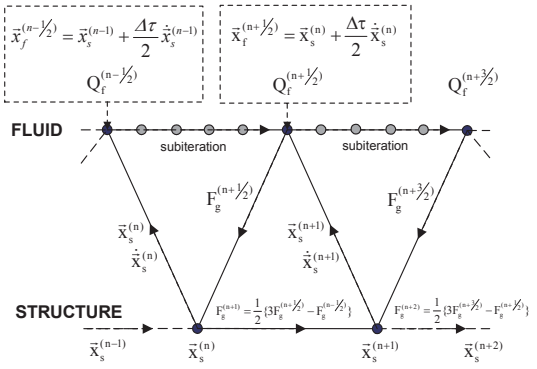

Fig. 1. Computation process of the second-order time-accurate staggered procedure.

Introducing the state vector {x} in order to efficiently perform the numerical integration, Eq. (12) can be recast into the first order form as

$$\{\dot{x}(t)\} = [A]\{x(t)\} + [B]\{u(t)\} \tag{12}$$

where

$$[A]=\begin{bmatrix} [0] & [I] \\ -[M_g]^{-1}[K_g] & -[M_g]^{-1}[C_g] \end{bmatrix}$$

$$[B]=\begin{bmatrix} [0] \\ [M_g]^{-1} \end{bmatrix} \tag{13}$$

$$\{x(t)\}=\begin{Bmatrix} \{q(t)\} \\ \{\dot{q}(t)\} \end{Bmatrix}, \quad \{u(t)\}=\begin{Bmatrix} \{0\} \\ \{Q(t)\} \end{Bmatrix}$$

Generally, to calculate the time response of Eq. (13) due to the initial conditions, external forces or control inputs are needed to analyze the behavior of the system. For nonlinear structural systems, a typical numerical technique like Runge-Kutta method can be commonly used but for linear structural systems we can use other approaches. One of the most robust and fast techniques for the linear system analysis can be derived from the assumption of setting the external force or control input constant, called zero order hold, during a certain small interval of time marching process. Thus, we can use the accurate analytical form of the solution obtained through the Laplace transform and inverse transform processes as

$$\{x(t)\} = e^{[A]t}\{x(0)\} + \int_0^t e^{[A](t-\tau)}[B]\{u(\tau)\}d\tau \tag{14}$$

The solution of Eq. (14) can be obtained numerically by replacing the continuous system by a discrete time system. Considering a computational time interval so that $n\Delta t < t \le (n+1)\Delta t$, and through the useful matrix manipulation for the integration of transition matrix, Eq. (14) can be derived as the following closed form:

$$\{x\}^{n+1} = e^{[A]\Delta t}\{x\}^n + [A]^{-1}\left(e^{[A]\Delta t} - I\right)[B]\{u\}^n \tag{15}$$

Then Eq. (15) can be effectively integrated in time to predict the modal displacement and velocity as presented in Ref.11.

The computed natural vibration mode shapes are interpolated into the aerodynamic grid points using the surface spline methods. A surface spline method can map the structural model into the

aerodynamic model. Unlike structured grid system, the unstructured aerodynamic grids automatically generated from a grid solver can hardly give ideally symmetric distributions on the object surface. In this study, thin-plate spline (TPS) technique is adopted. The global natural vibration mode shapes interpolated on the surface mesh of aerodynamic grid can be effectively displayed by the post-combination process using a general purpose plotting program. Recent useful information for several numerical spline techniques with numerical experiments can be found in Ref.12.

4. Multi-Disciplinary Aeroelastic Optimization

Typical frequency-domain flutter analyses technique based on p-k flutter method can be used to efficiently determine the flutter speed of the given wing configuration. The eigenvalue problem for classical flutter equation based on the p-k method can be written as follows:

$$\left([M_g]p^2+[C_g]p+[K_g]-\frac{1}{2}\rho U^2[A(M,k_b)]\right)\{\overline{q}\}=0 \qquad (16)$$

where p is the eigenvalue defined by $\rho=\omega(\gamma\pm i)$, ω is circular frequency, γ is transient decay rate coefficient, and $[A]$ is the generalized aerodynamic influence coefficient (GAIC) matrix of complex form as a function of Mach number M and reduced frequency k_b. The GAIC matrix can be calculated using linear subsonic doublet-lattice method, supersonic doublet-point method and transient pulse method (TPM) based on unsteady CFD aerodynamics. The numerical validation of the present flutter analysis method can be found in Refs.13-15.

Genetic algorithm is an optimization technique based on concepts of natural evolution and revolves around genetic reproduction processes and survival of the fittest strategies with some randomization or mutation. During the evolution, individuals with higher fitness will have a higher probability to survive and gradually dominate the population as the individuals with lower fitness die off. The micro genetic algorithm (mGA) is employed in this study as an alternative way to reduced the computational time compared to the classical genetic algorithm. In the micro genetic algorithm, jump and creep mutation processes are not required because the new generation process of population restarts whenever the diversity is lost. During the evolution, individuals with higher fitness tend to have higher probability to survive and gradually dominate the population as the individuals with lower fitness die off. The optimization model used in the generic algorithm can be represented by

Maximize $F(x)$:

$$\text{subject to} \quad \begin{aligned} & x\in\{A|(\theta_1,\theta_2,...,\theta_i)\}, \\ & \theta_i\in[0,\pm30,\pm45,\pm60,90] \end{aligned} \qquad (17)$$

where F(x) is the objective function and is the flutter dynamic pressure defined by $q=1/2\ \rho V_f^2$ and V_f is the flutter speed. The ply orientation angles are used as the design variables (x) in the algorithm to give the maximum flutter dynamic pressure.

Figure 2 shows the present multidisciplinary computation procedure based on the coupling technique among genetic algorithm, finite element and aeroelastic analysis system.

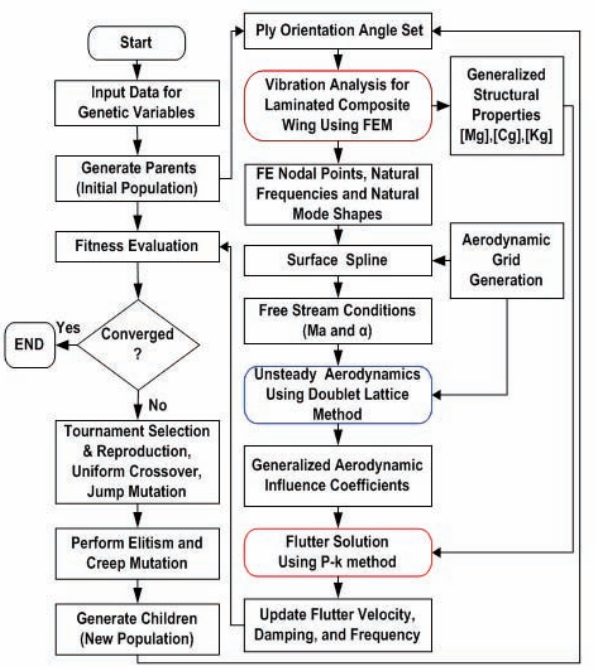

Fig. 2. Computational road map for the flutter optimization of laminated composite wings.

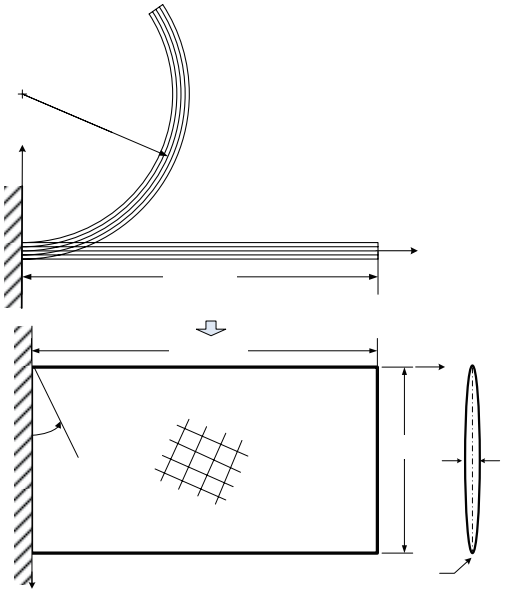

Fig. 3. Configuration of flat and curved composite wing.

5. Results and Discussion

In order to achieve strong potential for the practical application to realistic wing structures, the numerical algorithm and computational analysis system is practically designed. Developed aeroelastic computation system can be integrated with inhouse code or commercial finite element programs for linear and nonlinear composite structures. In this study, structural dynamic analyses of laminated composite curved wing models have been conducted using the MSC/NASTRAN (Ver.2005) which is a well-known and fully verified commercial finite element program. The curved wing structure is modeled using quadrilateral (CQUAD4) plate element with PCOMP entry to impose the composite material properties. The geometric configuration of the present curved wing

model is presented in Fig.3.

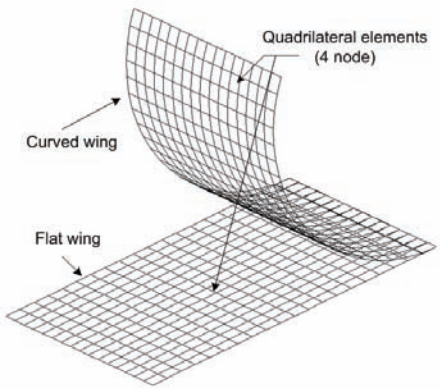

Fig. 4. Finite element models of flat and curved wing structures.

Figure 4 shows the corresponding finite element models for composite wings. The root chord of the wing is fixed in order to impose structural boundary conditions. The composite material properties used here are E_1=138 GPa, E_2=9.7 GPa, G_{12}=5.5 GPa, ν_{12}=0.28, ρ=1,543 kg/m^3 and ply thickness is 0.125 mm. The total number of plies is assumed as 32 and among them 24 inner plies can be changed according to the computational iteration coupled with the genetic algorithm. The lamination sequence is practically assumed as a symmetric lamination of $[0/90/45/-45/...\theta_{12}...]_s$. The variable angles of sets are practically selected based on the combination of 0°, 30°, 45°, 60°, and 90° ply orientations which is measured clockwise from the x-axis line. Symmetric flow boundary condition on the x-z plane is assumed for the unsteady aerodynamic analysis. The flight condition is assumed as sea-level with the free stream Mach number of 0.7.

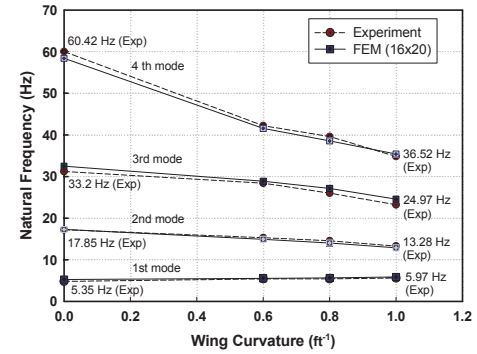

(a) Isotropic spanwise curved wing

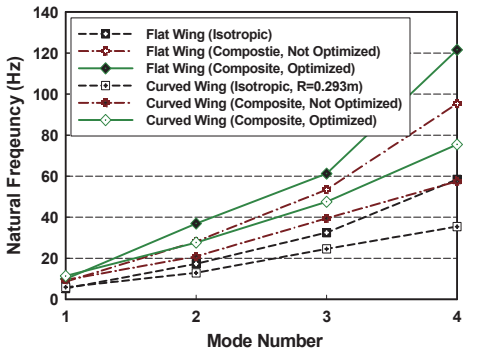

(b) Composite flat and curved wings

Fig. 5. Comparison of natural frequencies.

In the application of genetic algorithms, the variable ply angles considered is expressed in binary number such as: [0]=000, [30]=001, [-30]=010, [45]=011, [-45]=100, [60]=101, [-60]=110, and [90]=111. Numerical computations have been conducted using a server computer: Intel Pentium-D Processor 3.0 GHz, 2 GB DDR2 RAM and 240 GB HDD. The total run-time of the converged solution for each case using the standard genetic algorithm is about 33 hours for 20,000 iterations but the total run-time using the micro genetic algorithm is just about 1.67 hours for 1,000 iterations. One of the parameter sets used for micro GA is that the population size is 5, number of children is 1, crossover probability is assumed as 0.5, and elitism concept is used.

Figure 5 represents the comparison of natural frequencies for the isotropic and composite wing models. For the isotropic curved wing model presented in Fig.5(a), calculated natural frequencies show very good agreement with the experimental data[16]. For composite wing models, comparison of natural frequencies is given in Fig.5(b). Here, it is found that the natural frequency of curved wing model is generally lower than that of the flat wing model. Furthermore, natural frequencies for optimized composite wing models to achieve a maximum flutter dynamic pressure are higher than those of not optimized composite wing models.

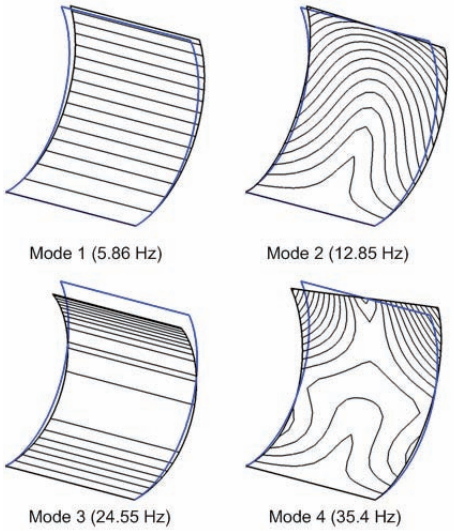

(a) Isotropic

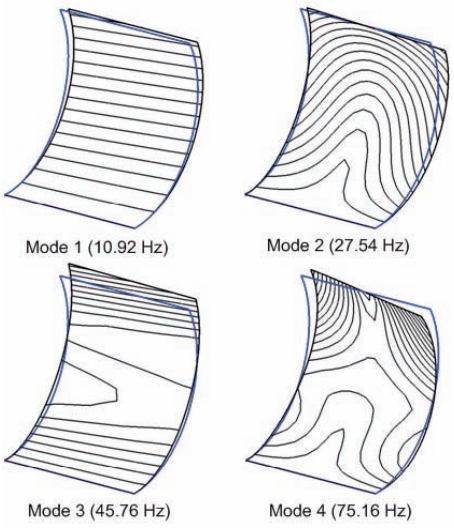

(b) Composite (Optimized)

Fig. 6. Comparison of natural mode shapes.

Figure 6 shows the comparison of natural vibration modes between isotropic and composite curved wings. For the isotropic

curved wing model, mode 1 is a typical first bending mode, mode 2 is a first torsion mode, mode 3 is a second bending model, and mode 4 is a second torsion model. The natural mode shapes of the optimized composite curved wing model are similar with those of isotropic model. However, it can be noted that the mode shapes of composite curved wing model has some combination of bending-torsion mode.

Table 1 Comparison of optimized flutter solution

Model Case	Stacking Sequence	Flutter Dynamic Pressure (kPa)	Flutter Freq. (Hz)
Isotropic Curved wing	N/A (A1 6061-T6)	2.58	9.72
Not Optimized	[0/90/45/-45/…**θ**…]s **θ** = 0/0/0/0/0/0/0/0/0/0/0/0	7.15	15.92
Optimized Using Standard GA	[0/90/45/-45/…**θ**…]s **θ** =45/45/45/-45/-45/-30/45/60/-60/-60/-30/30	16.47	20.43
Optimized Using Micro GA	[0/90/45/-45/…**θ**…]s **θ** =45/45/60/-45/-60/45/-45/45/-30/90/30/45	16.48	20.62

Computational results for optimum flutter design are summarized in Table 1. It is shown that the optimized flutter dynamic pressures are extremely higher than the case of the isotropic model under the condition of the same structural weight and aerodynamic shape. Flutter dynamic pressure of the isotropic material case is just 2.58 kPa. The flutter dynamic pressure of the initial composite wing models (flat and curved configuration) are higher than the case of the isotropic material model under the same weight and shape condition. This result basically indicates the benefits of composite material properties and characteristics compared to the isotropic materials. Moreover, the flutter dynamic pressure of optimized composite wing is 6.4 times greater than that of the isotropic wing model. Optimized results practically show that nearly same maximum flutter dynamic pressure by standard genetic algorithm can be also obtained using the efficient micro genetic algorithm.

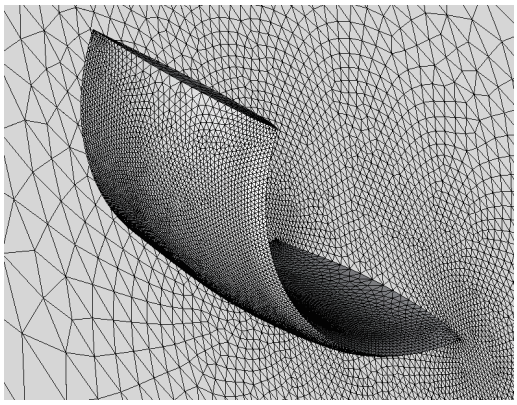

Fig. 7. Computational grids used for unsteady aerodynamic computations for flutter analyses.

Computational grid used for unsteady aerodynamic calculations using three-dimensional Euler code with deforming grid algorithm is presented in Fig.7. The grid is carefully stretched and distributed in order to decrease the total number of volume and increase the numerical accuracy. Here, whole computational grid domain is composed of about 200,000 tetrahedrons.

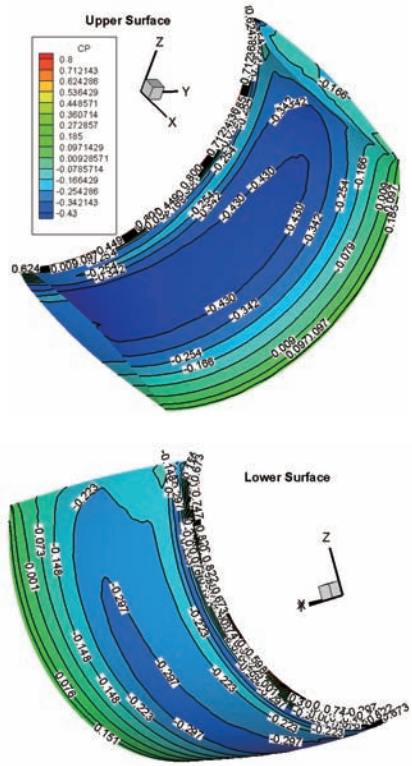

Fig. 8 Comparison of surface pressure distribution at the Mach number of 0.7.

Figure 8 represents the comparison of pressure distribution on the upper and lower wing surfaces. It is noted that although the present curved wing has a symmetric airfoil section such as NACA 65A010, the pressure distributions on the upper and the lower wing surfaces are different because of its spanwise curvature effect. For the isotropic wing model, experimental flutter test data[16] is available. The verification of the present computational flutter analysis for the curved wing model is presented in Table 2. The calculated flutter dynamic pressure and frequency using the developed computational program show good agreements with the experimental data.

Table 2 Comparison of flutter dynamic pressure and flutter frequency

Model	Experiment		Present (CFD/CSD)	
	q_F (kPa)	f_F (Hz)	q_F (kPa)	f_F (Hz)
Curved wing (Isotropic)	2.38	9.4	2.16	9.1

On the other hand, to account for physical aspect of structural responses for both the isotropic and composite curved wing models, verified advanced computational method based on the time-domain approach is also applied. Figure 9 shows the comparison of dynamic aeroelastic responses for the isotropic curved wing and the optimized composite wing models. For the response case of the composite curve wing model, one of the optimized laminations presented in Table 1 is considered: $[0/90/45/-45/45/45/60/-45/-60/45/-45/45/-30/90/30/45]_s$. Here, one can see that the maximum static aeroelastic defection of the isotropic curved wing is about -0.035 m for the dynamic pressure of 2.2 kPa while the maximum deflection of the composite curved wing is just about -0.022 m even for three times higher dynamic pressure level. Moreover, the dynamic response of the isotropic curved wing is clearly unstable for the low dynamic pressure level of 2.2 kPa. However, the optimized composite wing model which

has the same structural weight compared to that of the isotropic curved wing still shows the stable dynamic responses even for the high dynamic pressure level of 6.13 kPa. This result clearly indicates that the flutter dynamic pressure of a curved missile fin can be significantly increased using laminated composite materials.

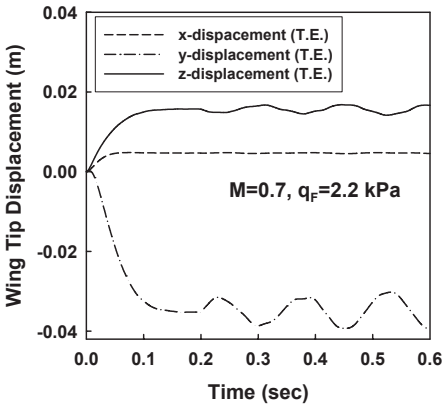

(a) Isotropic curved wing

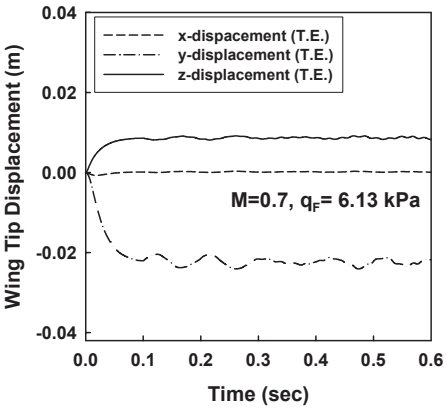

(b) Optimized composite wing

Fig. 9 Comparison of dynamic aeroelastic responses at the wing tip.

6. Concluding Remarks

Advanced computational methods for multi-disciplinary aeroelastic analysis are introduced in this article. The developed analysis system was based on the advanced numerical techniques such as CFD, CSD, FEM and parallel processing. Also, the design studies of aeroelastic tailoring were conducted on the laminated composite curved wing configuration. Using the developed analysis system, dynamic aeroelastic behaviors of a composite curved wing configuration were simulated in compressible flow. As computational demonstrations, the effects of ply orientation and stacking sequence on the flutter stability have been investigated and compared with the case of isotropic curved shell model with the same structural weight. The present results indicate that aeroelastic stability of a curved missile fin can be significantly increased using optimized composite lamination under the same design weight condition.

Acknowledgements

This work was partially supported by the 2nd Stage BK21 program and the Agency for Defense Development under the contact of UD060023AD. The authors would like to acknowledge the supports.

References

1) Weisshaar, T.A. : Aeroelastic Tailoring of Forward Swept Composite Wings, *Journal of Aircraft*, **18** (1981), pp.669-676.
2) Lottai, I. : Flutter and Divergence Aeroelastic Characteristics for Composite Forward Swept Cantilevered Wing, *Journal of Aircraft*, **22**, No. 11, (1985), pp.1001-1007.
3) Georghiades, G.A., Guo, S., and Banerjee J.R. : Flutter Characteristics of Laminated Wings, *Journal of Aircraft*, **33** (1996), pp.1204-1206.
4) Eastep, F.E., Tischler, V.A., Venkayya, V.V., and Khot, N.S. : Aeroelastic Tailoring of Composite Structures, *Journal of Aircraft,* Vol. **36** (1999), pp. 1041-1047.
5) Kim, D.H., and Lee, I. : Nonlinear Flutter Characteristics of a Composite Missile Wing in Transonic and Low-Supersonic Flows, *Journal of Aircraft*, **39** (2002), pp.889-892.
6) Guo, S., Banerjee, J.R., and Cheung, C.W. : The Effect of Laminate Lay-Up on the Flutter Speed of Composite Wings, *Journal of Aerospace Eng*, **217** (2003), pp. 115-122.
7) Kim, D.H., and Lee, I. : Static Aeroelastic Optimization of a Composite Wing Using Genetic Algorithm, 7th International Conference on Composites Engineering, ICCE/7, July 2-8 (2000), Denver Colorado, USA.
8) Holmes, D. G., and Connell, S. D. : Solution of the 2D Navier-Stokes Equations on Unstructured Adaptive Grids, AIAA Paper 89-1932 (1989).
9) Bruner, C., "Parallelizations of the Euler Equations on Unstructured Grids," *Ph.D. Thesis, Department of Aerospace Engineering, Virginia Polytechnic Institute and State University* (1996).
10) Karypis, G., and Kumar, V., "Analysis of Multilevel Graph Partitioning," *TR 95-037*, *Department of Computer Science, University of Minnesota*, 1995.
11) Kim, D. H., Park, Y. M., Lee I. and Kwon O. J. : Nonlinear Aeroelastic Computation of a Wing/Pylon/Finned-Store Using Parallel Computing, *IAA Journal*, **43** (2005), pp.53-62.
12) Smith, M. J., Cesnik C. E. S., Hodges, D. H., and Moran, K. J. : An Evaluation of Computational Algorithms to Interface between CFD and CSD Methodologies, AIAA Paper 96-1400-CP, (1996), pp.745-754.
13) Kim, D. H. and Lee, I., "Transonic Flutter Analysis for 3D Wing using Transonic Small Disturbance Equation," *Journal of The Korean Society for Aeronautical and Space Science*, **26** (1998), pp.73-82.
14) Kim, D. H. and Lee, I. : CFD-Based Matched-point Linear and Nonlinear Flutter Analysis of Sweptback Wings in Transonic and Supersonic Flows, Computational Fluid Dynamics Journal, **11** (2002), pp.35-49.
15) Kwon, H. J., Kim D. H., and Lee, I., "Frequency and Time Domain Flutter Computations of a Wing with Oscillating Flaperon Including Shock Interference Effects," *Journal of Aerospace Science and Technology*, **8**, (2004), pp. 519~532.
16) Rivera, J. A. Jr. : Experimental and Analytical Investigation of the Effect of Spanwise Curvature on Wing Flutter at Mach Number of 0.7, Langley Research Center, NASA TM 4096 (1989).